Integration of an Equivalent Aperture Method into Full-wave Electromagnetic Simulation of Airborne Radomes

Benjamin L. Cannon [1] and Jared Williams Jordan [2]

[1] Nuvotronics Inc., Durham, NC 27703, USA
bcannon@nuvotronics.com

[2] Raytheon Missile Systems, Tucson, AZ 85756 USA
jaredwilliamsjordan@gmail.com

Abstract ─ A method is provided for performing efficient, accurate, full-wave electromagnetic simulations of airborne radomes by representing the enclosed antenna with an equivalent aperture field distribution. In this case, the antenna and radome problems are essentially decoupled, and fine meshing details in the antenna region of the problem are eliminated. The equivalent aperture governing equations are discussed, and an algorithm for forming a representative aperture field distribution from far-field radiation patterns is provided. The success of the equivalent aperture method is demonstrated via an example problem. Equivalent aperture results are compared to full-wave simulations of a corresponding fully-detailed slot array antenna. For both the equivalent aperture and corresponding slot array antennas, a 2:1 fineness ratio tangent ogive radome with dielectric constant of 7 and metallic tip is simulated to determine the effects on radiation patterns, loss, and boresight error. Radome insertion loss agreement is achieved to within 0.3 dB or better and boresight error agreement is achieved to within 0.05 deg or better in both elevation and azimuth scan planes for a significantly detuned radome wall. Both transmit-mode and receive-mode formulations of the full-wave radome analysis and their appropriate uses are described.

Index Terms ─ Airborne radomes, aperture antennas, boresight error (BSE), Fourier transform, Lorentz reciprocity, monopulse radar.

I. INTRODUCTION

The simulation of radome effects on an enclosed radar antenna has been a topic of investigation for more than half of a century. The analysis of sharp-nosed, airborne radomes is particularly challenging. These airborne radomes are often electrically large structures—with respect to the operating frequency of the enclosed radar—which can require large amounts of computational resources to solve. Additionally, this class of radomes can often be considered electrically complex, particularly in the sharp-nosed tip region of the radome where the geometry does not appear locally flat and diffractive effects can dominate the electromagnetic interactions. For these two reasons, airborne radome modeling still remains an ongoing topic of investigation, and a universally accepted modeling technique has yet to exist.

Computational resources have improved drastically over the years, allowing for larger and more complicated antenna and radome simulations to be performed. As a result, the techniques used to model large, complicated radomes have evolved, with the fidelity of simulations being primarily limited by the computational resources available to the design engineer.

The first methods that were developed for radome analysis were based off of geometric optics (GO) [1-4], or ray-tracing, which is a high-frequency approximation method for analyzing the distortion of electromagnetic energy propagating through the radome. Bundles of rays are tracked as they propagate through and bounce off of the inner radome surface. This ray-optical approximation is typically based off of analytic Fresnel transmission and reflection coefficients [5] for planar slabs of infinite extent and therefore yields relatively quick results. Radome effects over entire scan spaces for both electrically and mechanically scanned arrays can be solved for in only a few minutes. This approach is particularly advantageous for modeling multi-layer structures because radome transmission and reflection coefficients can be determined by cascading 2x2 ABCD transmission line matrices for each of the layers [6]. However, the GO approximation does not fully capture the distortion of electromagnetic waves due to the radome, especially in the sharp-nosed tip region of the airborne radome where the geometry of the radome does not appear locally flat.

Over the years, advances have been made to

increase the fidelity of high-frequency approximation methods. Physical Optics (PO) methods and Aperture Integration Surface Integration (AiSi) methods [7-12] were developed to treat monolithic and layered radomes as scattering objects. In both the PO and AiSi approximations, equivalent electric and magnetic "currents" induced on the radome surfaces are integrated to determine radome effects. In both cases, the currents can be approximated by the same Fresnel transmission and reflection coefficients that are used in GO approximations. Additional advancements have been made in comprehending diffractive tip effects by hybridizing high frequency approximation methods with full-wave method [13, 14].

While radome simulation accuracy has indeed been increased as simulation fidelity is improved, all of the aforementioned approaches are at a fundamental level an approximation to the true electromagnetic wave interactions that take place in an antenna/radome system. Present-day computing capabilities have now permitted full-wave field solutions of certain radome geometries that are not too large or too complex. Commercially available software packages contain fast, accurate solvers which generate numerical solutions to Maxwell's equations for arbitrary, complex geometries [15-17].

Presented in this paper are the results of full-wave simulations in CST's commercially available time-domain solver, modeling the effects of a sharp-nosed airborne radome on a mechanically gimbaled seeker antenna. A case study is presented where a slotted array antenna sits in close proximity to a high fineness ratio radome with a sharp metallic tip. The seeker antenna is then replaced by an equivalent aperture field distribution that was derived from the far-field radiation patterns of the slotted array antenna. The use of an equivalent aperture to represent the seeker antenna eliminates the fine meshing details that are often required for complicated radiating elements and feeding structures (resonant cavities, power dividers/combiners, layer-to-layer transitions, etc.). The approximations that exist when using an equivalent aperture representation of the seeker antenna will be described.

By comparing results from a full-wave radome simulation that includes a physical antenna model to another full-wave radome simulation with a representative equivalent aperture, one can isolate and study the impact of decoupling the antenna and the radome. Additionally, there are benefits towards using full-wave simulation results as the basis for quantifying the accuracy of another proposed modeling technique instead of measured data. Firstly, expensive manufacturing of antenna and radome test articles and test facilities are avoided. Secondly, measurement errors associated with antenna and radome ranges are removed. Finally, accounting for discrepancies between the manufactured benchmark test articles and nominal simulation models is unnecessary.

II. RADOME/ANTENNA PROBLEM UNDER INVESTIGATION AND THEORETICAL BACKGROUND

The radome and antenna system under evaluation is shown in Fig. 1. The antenna diameter is 10 in and consists of 4 quadrants, each containing 17 half-wavelength resonant slots [18] designed for operation at 7 GHz. Each slot is individually fed by a WR-137 waveguide located behind the ground plane. The radome is a tangent ogive with an approximate fineness ratio of 2:1, inside base radius of 11 in, and an inner length of 22 in. The radome gimbal center is positioned 4 in into the radome from its base. The plane that the slots reside in is located 1 in from the gimbal center. The edge of the antenna is less than 0.25 in (15% of a freespace wavelength at 7 GHz) from the inside of the radome. The top 1 in of the radome is a sharp metal tip, modeled as a perfect electric conductor (PEC). The radome shell is 0.3 in thick and is constructed from a lossless dielectric with a relative permittivity of 7. The thickness of the radome wall was intentionally chosen to provide a detuned response at the operating frequency of 7 GHz to demonstrate the presented modeling methodology in a circumstance where significant bounce energy exists.

The normal of the antenna faceplate is directed along the positive z-axis and the radiating slots are y-polarized. The elevation plane is defined as the YZ plane, and the azimuth plane is defined as the XZ plane. The radome is gimbaled about the gimbal center while the antenna is fixed and results will be presented as such.
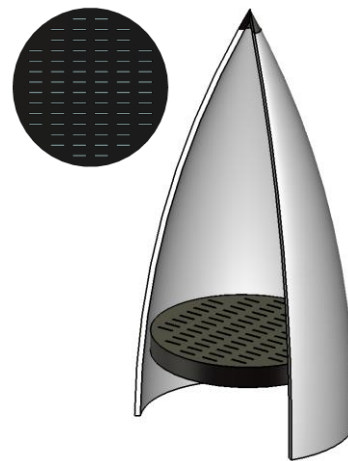

Fig. 1. Radome and antenna geometry under evaluation with a portion of the radome cut away for visual access to the antenna. An array of 68 half-wavelength resonant radiating slots is in close proximity to the radome.

Far-field radiation patterns, antenna boresight transmission loss and boresight errors are modeled using two different simulation methodologies. In both cases, simulations are performed in CST's time-domain solver based on the Finite Integration Technique (FIT). Firstly, the entire radome and antenna are simulated together using the previously provided parameters. By modeling the radome and antenna together the mutual coupling between these two entities is fully captured. The results from these simulations will be considered "truth" for the purpose of this paper, and henceforth be the standard by which we compare the proposed modeling method. As stated previously, it is convenient to allow a simulation to represent "truth" rather than a measured result as it eliminates any uncertainties in both the measurement system and the device under test. The second design methodology replaces the antenna with an equivalent aperture defined by representative fields or currents with no physical scattering object present. As a result, this method does not capture mutual coupling between the seeker antenna and radome. For this approximation to be valid, little energy propagating from the seeker antenna should bounce off the radome and couple back into the antenna and re-scatter off the antenna. Such interactions are fully captured in the first simulation methodology. Moneum et al. [13] believed this mutual coupling to be small for well-tuned radomes of this shape. The presented antenna/radome system under investigation aims to demonstrate the validity of this approach for a radome of this size/shape, even when the radome wall is significantly detuned.

The notion of using an equivalent aperture to represent an antenna is not new, but rather an old and well-understood concept [19]. The significance of what is presented here is the use of this method in conjunction with a full-wave radome solution that can accurately quantify the validity of this approach for radome design and analysis. Furthermore, the equivalent aperture method is applied to an intentionally detuned radome, which is a scenario that often yields unsatisfactory results in high-frequency approximation methods for radome analysis.

It is well-known that for large (many wavelengths in diameter), well-collimated antennas, one can perform a 2D Fourier Transform of the antenna's far-field radiation pattern to generate a well-representative equivalent aperture plane field distribution, which if inverse transformed, would reconstruct the original far-field pattern [20]. This method requires both the magnitude and phase of the far-field data for uniqueness. It is clear to see from (1) and (2) that the equivalent aperture field, $F(x,y)$ is related to the far-field response $U_p(k_x,k_y)$ by a two-dimensional Fourier

transform, where k_x (3) and k_y (4) are the x and y components of the free space propagation vector $\mathbf{k}$ (5). The far-field response is normalized by the freespace scalar Green's function, removing the amplitude and phase dependence associated with absolute far-field data;

$$F(x,y) \approx \iint_{k_y k_x} f(k_x,k_y)e^{-j(x \cdot k_x + y \cdot k_y)}dk_x dk_y, \qquad (1)$$

$$f(k_x,k_y) = \frac{-j\lambda U_p(k_x,k_y)}{\dfrac{e^{-jkR}}{R} \cdot (1+\cos(\theta))}, \qquad (2)$$

$$k_x = k\sin(\theta)\cos(\phi), \qquad (3)$$

$$k_y = k\sin(\theta)\sin(\phi), \qquad (4)$$

$$|\mathbf{k}| = \frac{2\pi}{\lambda}. \qquad (5)$$

The equivalent aperture approach is a high-frequency approximation, and for the size of the antenna under consideration it is applicable. The method starts with the acquisition of measured or simulated far-field radiation patterns for the antenna under evaluation in the absence of a radome. In this specific case study, simulated far-field patterns were computed utilizing the full-wave antenna-only model where the four quadrants are individually and simultaneously excited. The far-field radiation patterns are then Fourier transformed to form equivalent aperture field distributions. Because only propagating-mode information from the far-field is initially provided to the Fourier transform, this is an inversion problem.

Since the far-field data does not contain evanescent mode information, the equivalent aperture derived from the propagating mode far-field data is initially not a good representation of the antenna and is lacking in its ability to accurately model the antenna's near-fields. Correctly modeling the aperture near-field is imperative when the antenna is in close proximity to the radome. In an effort to reconstruct the lost evanescent mode energy, an extrapolation algorithm was implemented [19]. The method requires as an input a user-defined diameter of the resulting equivalent aperture. Future research could focus on non-circular apertures, and determining the optimal outer-aperture contour to be used in the extrapolation algorithm. The diameter used for this study was chosen to be equal to the ground plane diameter of the radiating slot antenna. The equivalent aperture should be as large as the physical extent of the antenna it is representing. Consequently, the original farfield pattern data must be sampled in fine enough increments to create an equivalent aperture with maximum extents larger than that of the physical antenna. The extrapolation algorithm is summarized as follows:

1) *Far-field data is Fourier transformed to create an equivalent aperture.*
2) *Aperture fields outside of a user-defined aperture diameter are removed.*
3) *The truncated aperture is inverse Fourier transformed to obtain its corresponding far-field data.*
4) *The newly created evanescent mode information from this far-field data is appended to the original far-field data.*
5) *Steps 1-4 are repeated until fields in the aperture plane have converged to a steady value.*

The aperture is flat and exists in a 2D plane. In general, because the Fourier transform operates on a scalar, this process must be repeated separately for the two orthogonal far-field polarizations to form the two orthogonal polarizations that fully define the tangential aperture fields.

The magnitude and phase for the initial antenna far-field simulation can be seen in Fig. 2 (a) and Fig. 2 (b), respectively. Ludwig's 3rd definition of co- and cross-polarization is utilized, and the co-polarized far-field radiation pattern is what is shown [21]. According to Ludwig's 3rd definition, the y-polarized radiating slot array in the absence of the radome produces a primarily co-polarized far-field response and very little cross-polarized energy exists. Full-wave solutions of the equivalent aperture behind the radome will fully comprehend the polarization distortion that the radome causes. By applying the two-dimensional Fourier transform to the co-polarized far-field response, the y-directed electric field distribution in the aperture plane is approximated as shown in Fig. 2 (c) and Fig. 2 (d). As stated previously, if the antenna under investigation had produced significant cross-polarized energy in the far-field, an additional transform would have been necessary to approximate the x-component of the electric fields in the aperture plane. The corresponding equivalent aperture magnetic fields are determined by applying the same relationship that exists between electric and magnetic fields under far-field conditions [22].

The implementation of (1)-(5) in conjunction with the extrapolation algorithm was successful in producing a 10 in diameter equivalent aperture surrounded by energy approximately -30 dB or lower from the peak aperture field value outside of the user-specified diameter. These fields outside the 10 in diameter aperture are removed prior to performing analysis with the radome. Containing the aperture energy into a diameter no greater than the original antenna is desirable for its use in applications where the radome is in close proximity to the employed antenna.
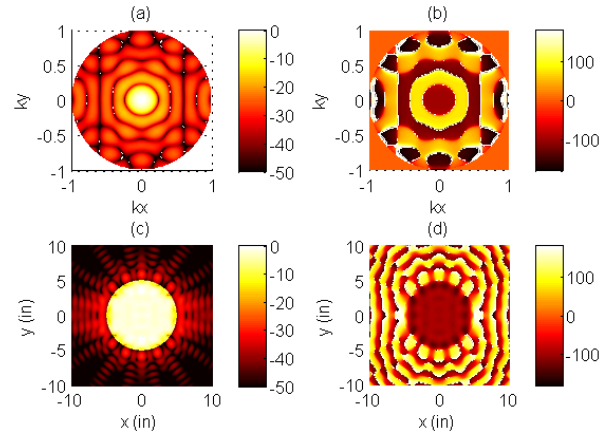

Fig. 2. Transformation of antenna far-field patterns to an equivalent aperture. (a) Normalized magnitude (dB) of antenna far-field in k-space. (b) Phase (deg) of antenna far-field in k-space. (c) Normalized magnitude (dB) of equivalent aperture. (d) Phase (deg) of equivalent aperture.

The resulting aperture field distribution can be utilized in two ways. Firstly, as a source to the radome problem where the radome scatters electromagnetic energy propagating from the aperture plane to the far-field, herein referred to as "transmit-mode." Alternatively, the fields can be utilized to receive energy from a plane wave passing through the radome by exploiting the Lorentz reciprocity integral provided in (6) [22] herein referred to as "receive-mode." $\mathbf{E_R}$ and $\mathbf{H_R}$ are the fields in the aperture plane due to the incident plane wave passing through the radome, while $\mathbf{E_T}$ and $\mathbf{H_T}$ are the equivalent aperture source fields. Because mutual coupling to the radome is neglected, these transmit and receive fields in the Lorentz reaction integral are approximate;

$$VR_{APER} = C\iint_{yx} (\mathbf{E_T} \times \mathbf{H_R} - \mathbf{E_R} \times \mathbf{H_T}) \cdot \hat{\mathbf{n}} \, dxdy. \quad (6)$$

The complex scale factor C in (6), is required for determining an absolute received voltage; however, this term is not necessary when only a relative or normalized voltage is needed, as is the case when determining radome boresight errors or relative transmission losses.

The antenna and associated equivalent aperture are divided into four equal quadrants as is done in a conventional monopulse tracking system. Sum and difference channels are formed by adding or subtracting the received or transmitted voltages for each of these quadrants from one another, as is provided in (7)-(9) where VR_{SUM}, $VR_{\Delta EL}$, and $VR_{\Delta AZ}$ are the received voltages for the formed sum, delta elevation, and delta azimuth channels, respectively;

$$VR_{SUM} = VR_{Q1} + VR_{Q2} + VR_{Q3} + VR_{Q4} , \quad (7)$$

$$VR_{\Delta EL} = VR_{Q1} + VR_{Q2} - VR_{Q3} - VR_{Q4} \ , \tag{8}$$

$$VR_{\Delta AZ} = VR_{Q1} - VR_{Q2} - VR_{Q3} + VR_{Q4} \ . \tag{9}$$

The loss due to the radome is calculated in (10) by comparing the formed sum channel transmission through the radome (7) to the case when the radome is not present, referred to as "Air Radome". Additionally, the elevation boresight error and azimuth boresight error are calculated in (11), (12), where S_{EL} and S_{AZ} are the monopulse slopes for the formed delta elevation and formed delta azimuth channels, respectively [23];

$$RadomeLoss_{dB} = 20 \log_{10} \left(\frac{VR_{SUM}(\text{Radome})}{VR_{SUM}(\text{Air Radome})} \right), \tag{10}$$

$$BSE_{EL} = \frac{1}{S_{EL}} imag \left(\frac{VR_{\Delta EL}}{VR_{SUM}} \right), \tag{11}$$

$$BSE_{AZ} = \frac{1}{S_{AZ}} imag \left(\frac{VR_{\Delta AZ}}{VR_{SUM}} \right). \tag{12}$$

In the section to follow, far-field radiation pattern results make use of the transmit-mode application of the aperture fields, while boresight radome loss and boresight error calculations utilize the receive-mode application of the aperture fields. Boresight radome loss and boresight error can also be calculated via transmit mode, but this requires the individual simulation of each of the aperture channels within the radome. By calculating these results using a receive-mode formulation, the radome simulation only needs to be run once per look direction with an incident plane wave source, and the Lorentz reaction integral can be utilized in post-processing to calculate the different aperture received voltages. It is important to note that in this method a full Lorentz reciprocity is not achieved as scattered fields from the radome back into the aperture plane are ignored. A transmit-mode simulation would be required to acquire such information. Furthermore, since the radome problem is only run once for each gimbal direction, numerous apertures can be analyzed independently and seamlessly integrated with the radome simulation results to quantify boresight radome loss and boresight error for various antennas.

III. RADOME MODELING RESULTS AND DISCUSSION

The equivalent aperture method is demonstrated by comparing far-field radiation pattern cuts along the elevation and azimuth planes at three radome gimbal directions of interest, using either the full antenna or the equivalent aperture as the radiation source within the radome under investigation. Each of the four curves within each far-field pattern figure are created by one of the four radiation scenarios: the full slot antenna by itself, the equivalent aperture by itself, the full slot

antenna enclosed by the radome, and the equivalent aperture enclosed by the radome. As stated previously simulation results including the full antenna (designated by solid lines) are considered to be "truth" and serve as the baseline to quantify the accuracy of the equivalent aperture method simulation results (designated by dashed lines).

Radiation patterns with the antenna looking out the radome nose are of particular interest since the tip is directly illuminated by the main beam of the antenna/aperture and diffractive effects are significant. The pattern comparisons along the elevation and azimuth planes are presented in Figs. 3 (a) and (b), respectively. One feature of primary significance is how much the detuned radome influences the main beam of the antenna. In this case study, there is approximately 2 dB of attenuation due to the radome; meaning almost forty percent of the original energy transmitted towards antenna/aperture boresight is now scattered in different directions. The energy lost from the main beam results in an overall increase in sidelobe levels.
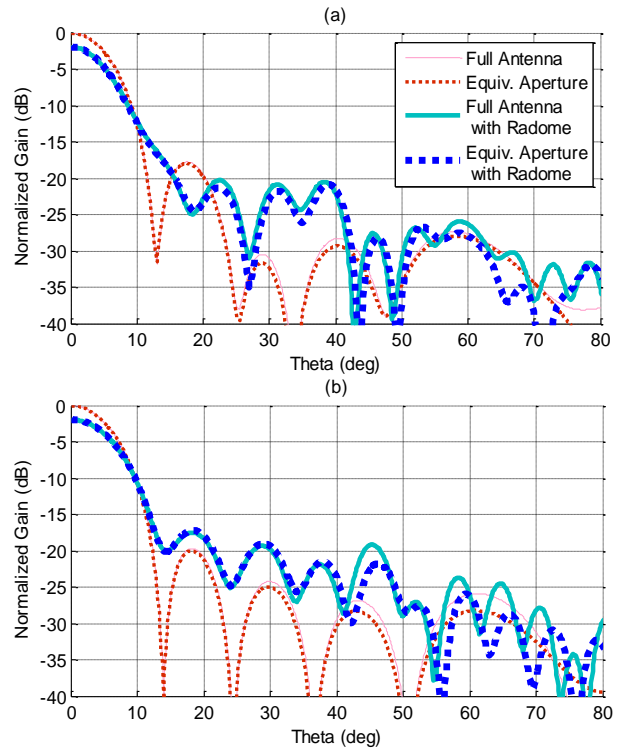

Fig. 3. Effect of radome on antenna/aperture far-field patterns where the radome is gimbaled 0 degrees in Azimuth and 0 degrees in elevation. (a) Far-field patterns in EL-plane. (b) Far-field patterns in AZ-plane. Patterns are normalized to peak antenna/aperture far-field value.

Even though the radome has such a dramatic effect on the radiation pattern of the antenna, it is clearly

shown that the equivalent aperture method is indeed applicable in predicting these RF radiation pattern perturbations. Peak gain is predicted to within small fractions of a dB for the main beam and first three sidelobes, and to within a few dB for a majority of the remaining low-energy sidelobes. This agreement is an indication that the coupling of energy back into the antenna is likely low for this radome shape, for this look-direction, even with its detuned thickness. Similar agreement between the two methods is witnessed in the azimuth plane.

Another radome gimbal angle of interest is 0 deg in azimuth and 20 deg in elevation. Excellent agreement between far-field patterns in the elevation plane can be seen in Fig. 4. The sidelobes are relatively unaffected by the presence of the radome at this gimbal angle, but significant deflection of the main beam is present, which is successfully predicted by the equivalent aperture simulations.
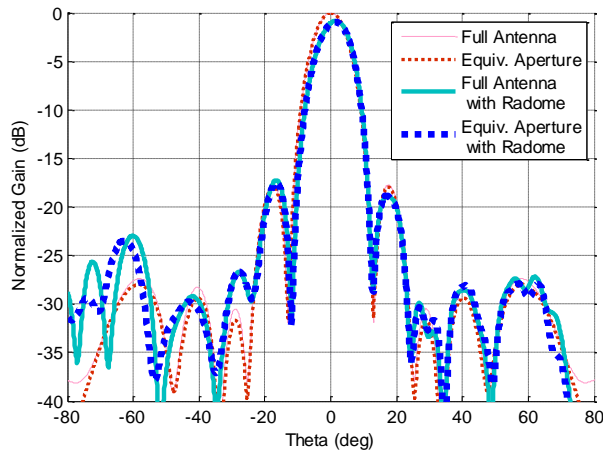

Fig. 4. Effect of radome on antenna/aperture EL-plane far-field patterns where the radome is gimbaled 0 degrees in Azimuth and 20 degrees in Elevation. Patterns are normalized to peak antenna/aperture far-field value.

The remaining radome gimbal angle of interest is 14 deg in azimuth and 0 deg in elevation. Here, a noteworthy phenomenon is successfully predicted and can be seen in Fig. 5. A bounce lobe—sometimes referred to as a flash lobe—has formed in the azimuth plane far-field pattern cut and is centered about 60 deg theta. Bounce lobes are a result of strong main beam reflections off the radome wall which coherently add to form a sidelobe of significant amplitude. This is a common occurrence for poorly tuned radomes which possess high fineness ratios.

Loss at antenna boresight is an important radome performance parameter and is difficult to appreciate in Figs. 3 – Fig. 5 due to their large vertical scale ranges.

With such a large scale it is very difficult to quantify how well the radome-induced loss is being predicted. That being the case, the radome loss at boresight for both the elevation and azimuth planes is presented in Fig. 6, where zero to half-power transmission is used as the plot's y-axis. It can be seen that using the aperture fields in receive mode, the deviation from our "truth" baseline is at most 0.2–0.3 dB which is approximately 2–4 % error in the far-field intensity prediction.
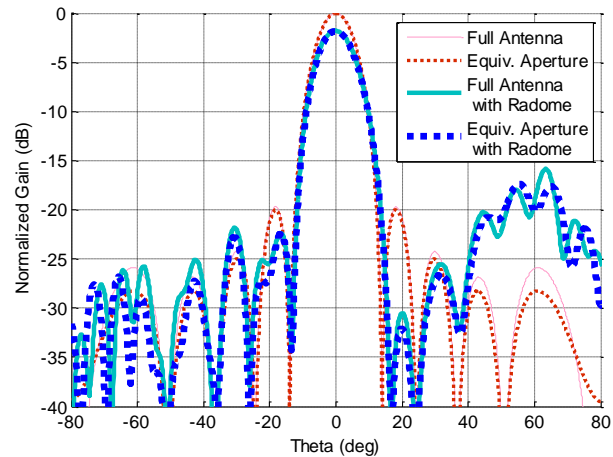

Fig. 5. Effect of radome on antenna/aperture AZ-plane far-field patterns where the radome is gimbaled 14 degrees in azimuth and 0 degrees in elevation. Patterns are normalized to peak antenna/aperture far-field value.
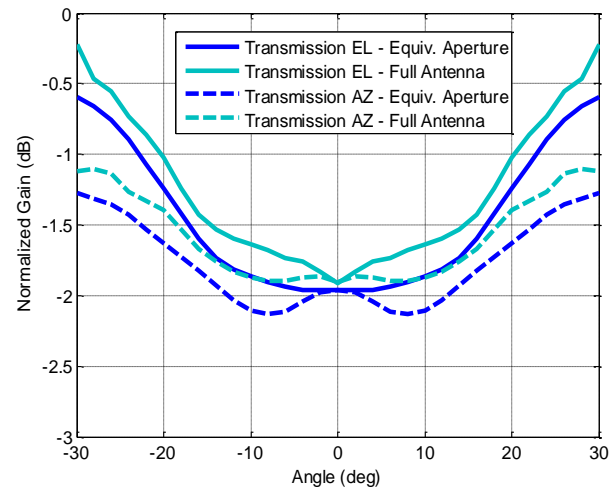

Fig. 6. Effect of radome on antenna/aperture bore-sight transmission as radome is gimbaled in the elevation/ azimuth plane. Transmission values are normalized to antenna/aperture bore-sight transmission.

Another radome performance characteristic often considered is the induced boresight error as a result of

the radome perturbing the magnitude and phase of energy as it propagates through the radome at varying incident angles and thicknesses. The results for both the elevation and azimuth plane boresight error can be found in Fig. 7. Excellent agreement is achieved between the two methods for both BSE AZ and BSE EL, indicating that the equivalent aperture has sufficiently represented the full seeker antenna in the radome simulation without including higher order effects that may exist due to mutual antenna and radome interactions.

With the presented modeling approach, an antenna/radome engineer can utilize the receive mode formulation to quickly compare several different antennas under the same radome. First, several different antennas can be simulated independently. Next, the effects of the radome on each different antenna's transmission and induced angle errors can be quickly quantified by performing an approximate Lorentz reaction integral. Conversely, if the radome engineer has the time and computation resources and requires more accurate results, radome loss and boresight error can be calculated in transmit mode; however, this will require up to N (i.e., number of aperture channels) simulations per antenna per radome gimbal direction and is no longer independent of the antenna(s) under consideration.
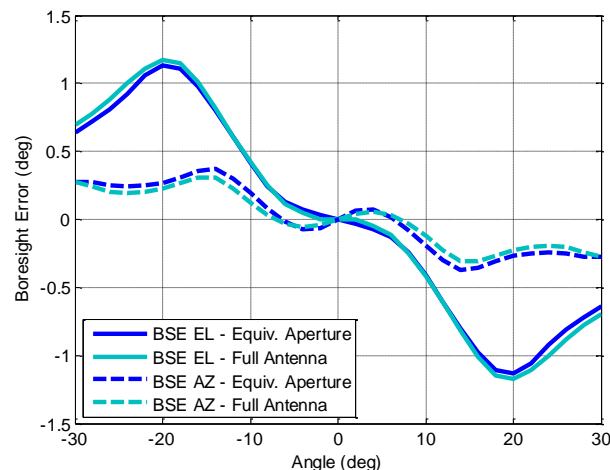

Fig. 7. Antenna/aperture bore-sight error as radome is gimbaled in the elevation/azimuth plane.

IV. CONCLUSIONS

There is a growing demand for accurate, full-wave modeling of radome induced angle errors, insertion loss, and effects on antenna patterns, while being mindful of computational resources and run time. The presented equivalent aperture method helps to bridge the gap between the speed of high frequency approximation solvers and the accuracy of full-wave modeling.

It is important to re-iterate that the equivalent

aperture that is formed via the presented transformation/extrapolation method is in no way specific to the radome. The aperture is formed from *antenna-only* radiation patterns and does not depend on the radome or its properties. As a result, the antenna and radome problems can be decoupled, simulated separately and combined seamlessly using the equivalent aperture receive mode to obtain accurate and efficient predictions of radome loss and boresight error. Furthermore, radiation pattern predictions using the equivalent aperture transmit mode are obtained without the additional cost of meshing the complex antenna structure behind the antenna, which results in significant cost savings in computer memory and runtime. This approach is valid for the sharp-nosed airborne geometry that was presented because little energy that scatters off the radome reflects back into the aperture plane.

REFERENCES

[1] G. K. Huddleston, H. L. Bassett, and J. M. Newton, "Parametric Investigation of Radome Analysis Methods," *Georgia Institute of Technology, School of Electrical Engineering*, 1980.

[2] G. Tricoles, "Application of ray tracing to predicting the properties of a small, axially symmetric, missile radome," *Antennas and Propagation, IEEE Transactions on*, vol. 14, no. 2, pp. 244-246, 1966.

[3] K. Siwiak, T. B. Dowling, and L. Lewis, "Boresight errors induced by missile radomes," *Antennas and Propagation, IEEE Transactions on*, vol. 27, no. 6, pp. 832-841, 1977.

[4] D. Burks, E. Graf, and M. Fahey, "A high-frequency analysis of radome-induced radar pointing error," *Antennas and Propagation, IEEE Transactions on*, vol. 30, no. 5, pp. 947-955, 1982.

[5] C. A. Balanis, *Advanced Engineering Electromagnetics*. New York, NY: John Wiley & Sons, 1989.

[6] D. M. Pozar, *Microwave Engineering*. John Wiley & Sons, 2009.

[7] C. D. Finlay, S. Gregson, R. W. Lyon, and J. McCormick, "SPIKE a physical optics based code for the analysis of antenna radome interactions," *In Radar Systems, 2007 IET International Conference on*, IET, pp. 1-5, 2007.

[8] H. F. Meng, W. Dou, and K. Yin, "Analysis of antenna-radome system at millimeter wave band," *In Millimeter Waves, 2008, GSMM 2008, Global Symposium on, IEEE*, pp. 380-383, 2008.

[9] T. Schuster and M. Sabielny, "REACH/PREACH—A physical optics based tool for simulation of radome effects on antenna patterns," *In Antennas and Propagation (EUCAP), 2012 6th European Conference on, IEEE*, pp. 3225-3229,

2012.

[10] D. Paris, "Computer-aided radome analysis," *Antennas and Propagation, IEEE Transactions on*, vol. 18, no. 1, pp. 7-15, 1970.

[11] D. C. Wu and R. Rudduck, "Plane wave spectrum-surface integration technique for radome analysis," *Antennas and Propagation, IEEE Transactions on*, vol. 22, no. 3, pp. 497-500, 1974.

[12] J. A. Shifflett, "CADDRAD: A physical optics radar/radome analysis code for arbitrary 3D geometries," *Antennas and Propagation Magazine, IEEE*, vol. 39, no. 6, pp. 73-79, 1997.

[13] M. A. Abdel Moneum, Z. Shen, J. L. Volakis, and O. Graham, "Hybrid PO-MoM analysis of large axi-symmetric radomes," *Antennas and Propagation, IEEE Transactions on*, vol. 49, no. 12, pp. 1657-1666, 2001.

[14] H. Meng and W. Dou, *Analysis and Design of Radome in Millimeter Wave Band*, Microwave and Millimeter Wave Technologies from Photonic Bandgap Devices to Antenna and Applications, Igor Minin (Ed.), ISBN: 978-953-7619-66-4, InTech, DOI: 10.5772/9054, 2010.

[15] CST Microwave Studio, Computer Simulation Technology, Darmstadt, Germany, www.cst.com

[16] HFSS ANSYS, High Frequency Structural Simulator, www.ansys.com

[17] Comsol Multiphysics, Comsol, Inc., Burlington, MA, www.comsol.com

[18] R. S. Elliott, *Antenna Theory and Design*. John Wiley & Sons, 2003.

[19] G. K. Huddleston, "Aperture synthesis of monopulse antenna for radome analysis using limited measured pattern data," *In SOUTHEASTCON'81; Proceedings of the Region 3 Conference and Exhibit*, vol. 1, pp. 350-354, 1981.

[20] S. Silver, *Microwave Antenna Theory and Design*. vol. 19, Iet, 1949.

[21] A. Ludwig, "The definition of cross polarization," *Antennas and Propagation, IEEE Transactions on*, vol. 21, no. 1, pp. 116-119, 1973.

[22] R. F. Harrington, *Time Harmonic Electromagnetic Fields*. McGraw-Hill Book Co., New York, 1961.

[23] D. J. Kozakoff, *Analysis of Radome-Enclosed Antennas*. Artech House Publishers, 2009.

Benjamin L. Cannon was born in McKeesport, PA in 1986. He received the B.S. degree in Electrical and Computer Engineering from Carnegie Mellon University, Pittsburgh, PA, in 2008 and the S.M. degree in Electrical Engineering from the Massachusetts Institute of Technology, Cambridge, MA in 2010. He worked as a Senior Electrical Engineer at Raytheon Missile Systems, Tucson, AZ (2010-2013), and is currently a Member of the Technical Staff at Nuvotronics, Inc., Durham, NC. He is interested in electromagnetic field and wave interactions with materials.

Jared Williams Jordan was born in Farmington, Maine on February 6, 1983. He received the B.S. degree in Electrical and Computer Engineering from University of Maine, Orono, ME, in 2005 and the M.S. degree in Electrical and Computer Engineering from University of Arizona, Tucson, AZ, in 2008. He has worked at Newpage Corporation as a Reliability Engineer (2005–2006) and at the University of Arizona as a Senior Research Engineer (2008–2010). He previously worked as a Senior Electrical Engineer at Raytheon Missile Systems, Tucson, AZ (2010-2014), and is currently an Associate Technical Staff at MIT Lincoln Laboratory, Lexington, MA in the Advanced Technology Division: RF Technology (group 86). is current research interests include antenna and radome analysis and design, computational electromagnetics and material characterization.